In Situ Gap-Mode Raman Spectroscopy on Single-Crystal Au(100) Electrodes: Tuning the Torsion Angle of 4,4′-Biphenyldithiols by an Electrochemical Gate Field

Li Cui,[†] Bo Liu,[‡] David Vonlanthen,[§] Marcel Mayor,[§,||] Yongchun Fu,[‡] Jian-Feng Li,[‡] and Thomas Wandlowski*,[‡]

[†]Institute of Urban Environment, Chinese Academy of Sciences, 1799 Jimei Road, Xiamen 361021, P. R. China
[‡]Department of Chemistry and Biochemistry, University of Bern, Freiestrasse 3, Bern CH-3012, Switzerland
[§]Department of Chemistry, University of Basel, St.-Johanns-Ring 19, 4056 Basel, Switzerland
[||]Institute for Nanotechnology, Karlsuhe Institute of Technlogy (KIT), P.O. Box 3640, 76021 Karlsruhe, Germany

Ⓢ Supporting Information

ABSTRACT: In situ gap-mode Raman spectra were acquired in an electrochemical environment on a single-crystal gold electrode employing a Au(100)|4,4′-biphenyldithiol (BPDT)|Au-NP(55 nm) sandwich assembly. This geometry enabled an investigation of the influence of an applied electrochemical gate field on the conformational changes in nanojunctions, such as the torsion angle (φ) of molecules. A linear correlation between the intensity ratio $I_{C=C}/I_{C_{ring}-S}$ and $\cos^2 \varphi$ in 4,4′-BPDT-type molecular junctions was established and subsequently utilized to estimate the potential dependence of the torsion angle of the "flexible" molecule **M1** at different potentials. The latter decreases as the potential (charge) becomes more negative, resulting in better $\pi-\pi$ coupling, which correlates with enhanced junction conductance. The demonstrated spectroelectrochemical strategy and the direct correlation of the spectroscopic results with (single) molecular conductance studies may guide the selection and elucidation of functional molecules for potential applications in novel nanodevices.

Self-assembled organic monolayers (SAMs) of organo(di-)thiols on gold surfaces have emerged as model systems for exploring fundamental aspects of the structure and functionality of organic thin films and monolayers.[1,2] In particular, the understanding and tuning of charge transport in nanoscale metal|molecule|metal junctions represent key issues in the realization of an electronics based on molecules.[3−6] Mesoscopic transport experiments with single molecules and molecular ensembles in different test beds (see the recent reviews in refs 3−8 and the literature cited therein) as well as electrochemical studies with redox proteins[9] or ferrocene covalently attached to electrodes via molecular linkers[10] have revealed that polyaromatic (di)thiols may act as efficient molecular wires and electron-transfer promoters.

However, the direct probing of structure and chemical changes in nanoscale molecular junctions upon application of an electric field is still a major challenge. Therefore, it would be highly desirable to develop strategies capable of identifying and characterizing the structures of molecules in these junctions and revealing relationships between molecular structure and

electrical properties or other functionalities. Current experimental strategies are based on inelastic electron tunneling spectroscopy (IETS)[11,12] and surface-enhanced Raman spectroscopy (SERS) in "on-edge",[13] electromigrated,[14] or nanoscale break junctions;[15] tip-enhanced Raman spectroscopy (TERS);[16] and various ensemble approaches involving the alignment of 10^3-10^{12} molecules in parallel between two conducting substrates.[17,18] While conventional SERS is limited to rough metallic or nanostructured surfaces,[19] the Raman scattering efficiency is greatly enhanced in nanosized gaps through excitation of localized surface plasmons.[14−16,20−24] A particular unique gap-mode configuration with high structural control has been achieved by depositing "plasmonic" gold nanoparticles (Au-NPs) with a narrow size distribution on top of organic monolayers adsorbed on atomically flat single-crystal metal surfaces.[21,25] This approach was extended recently by Li et al.[26] using Au-NPs covered with an inert silica shell to protect the SERS-active nanostructure from direct chemical interaction with the adlayer and/or the substrate surface.
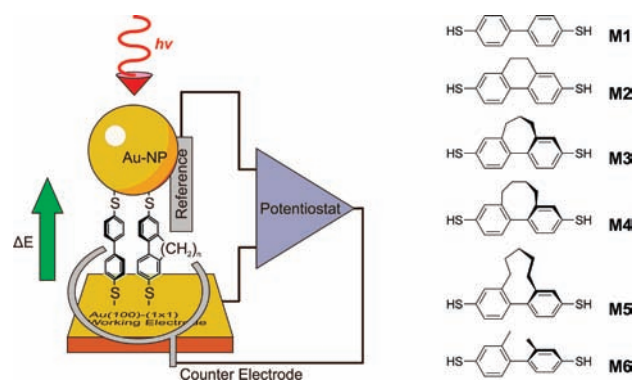

Figure 1. Schematics of the sandwich assemblies and the investigated 4,4′-biphenyldithiols **M1−6**.

In the present communication, we report the first electrochemical study of gap-mode Raman spectroscopy on an Au(100) single-crystal electrode in 0.05 M KClO$_4$ at pH 9. Employing the
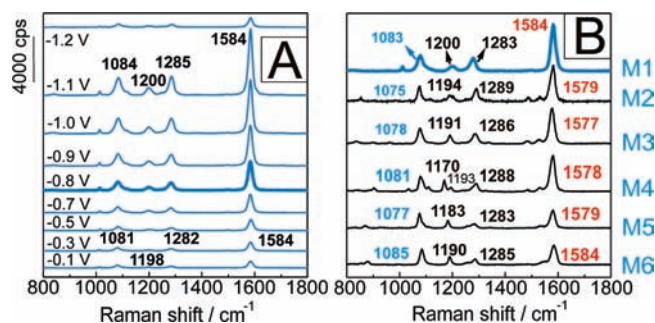
Figure 2. (A) Potential-dependent gap-mode Raman spectra of Au (100)-$(1 \times 1)|\mathbf{M1}|$Au-NP(55 nm) in 0.05 M KClO$_4$ (pH $\sim$9). (B) Corresponding Raman spectra of **M1** to **M6** at -0.8 V vs Ag/AgCl, normalized to the C$_{ring}$−S stretching band of **M1**. Excitation line, 632.8 nm; laser power, 0.15 mW; acquisition time, 5 s.

Figure 3. (A) Integrated intensity ratio I_{1580}/I_{1080} $(I_{C=C}/I_{C_{ring}−S})$ for **M1** vs potential from 0 to -1.1 V and -1.1 to 0 V. (B) $I_{C=C}/I_{C_{ring}−S}$ ratios for **M2**−**M6** vs potential from 0 to -1.0 V.

concept of "electrolyte gating"[27] to Au$(100)|4,4'$-biphenyldithiol (BPDT)$|$Au-NP(55 nm) junctions, we demonstrate electric-field-induced changes in the torsion angle between the two phenyl rings.

Recent single-molecule STM-based break junction experiments have shown that the conductance through p-NH$_2$-,[28] p-SH-,[29] and p-CN-substituted[30] biphenyls attached to gold contacts varies linearly with cos^2 φ, where φ is the torsion angle. The torsion angle between the two interconnected aromatic rings was controlled by "chemical tuning". In particular, in refs 29 and 30, attachment of alkyl chains of various lengths ("molecular straps") at the 2 and 2′ positions guaranteed minimum motion and conformational freedom of the bridge without changing the electronic character of the substituents and the length of the bridging molecules.

In order to address the role of an applied electric (electrochemical) field on φ in π-conjugated aromatic compounds, we performed in situ Raman spectroscopic measurements on 4,4′-BPDTs with "free" (**M1**) or (for internal reference) fixed (**M2**−**6**) torsion angles ranging between 17 and 79,7°[29,31] in a Au$(100)|4,4'$-BPDT$|$Au-NP(55 nm) configuration under electrochemical conditions. Figure 1 illustrates the experimental setup. The chosen sandwich structure represents an ensemble arrangement of parallel molecular tunneling junctions with nanometer-sized dimensions on a well-defined single-crystal electrode. The applied electrochemical potential controls the potential drop between the Au(100) and Au-NP(55 nm) electrodes (the "Helmholtz layer") and therefore resembles the bias voltage in a molecular conductance experiment.

The sandwich structure was created by first assembling the chosen 4,4′-BPDT molecules on an island-free Au(100)-(1×1) surface from 0.3 mM ethanol solution at 60 °C. Ensuring the absence of oxygen led to densely packed but disordered monolayers with one thiol group bound to the gold substrate and the biphenyl backbone tilted at angles of up to 40° with respect to the surface normal.[16,31,32] Next, $\sim$55 nm diameter Au-NPs that had been synthesized by citrate reduction of HAuCl$_4$ in aqueous solution[33] were dropped onto the Au$(100)|4,4'$-BPDT surface and dried in vacuum. The freshly prepared electrode was subsequently transferred into a custom-made spectroelectro-chemical cell for in situ gap-mode Raman experiments in a backscattering geometry. Further details concerning sample preparation and the experimental Raman setup are summarized in the Supporting Information (SI).

Identical results were obtained with nanoparticle films and well-dispersed nanoparticles (see the SI). In the latter case, the
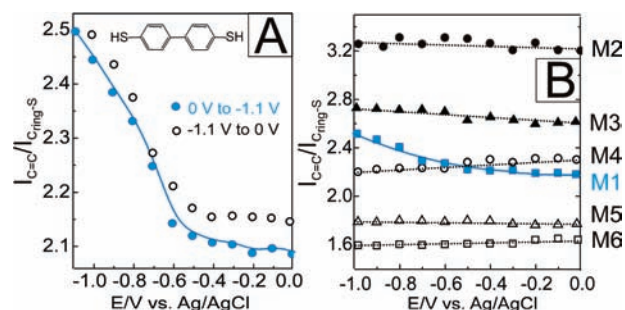
interparticle distance was much larger than the sphere−plane gap (i.e., the thickness of the organic monolayer). Therefore, one may expect that the dominant Raman gap modes are mainly excited between the Au-NP(55 nm) and the Au(100) plane.[16,21]

Figure 2A displays typical potential-dependent gap-mode Raman spectra recorded for Au$(100)|\mathbf{M1}$ in the presence of an Au-NP(55 nm) top layer upon excitation with 632.8 nm light from a He−Ne laser. Figure 2B compares the spectrum of **M1** with those of **M2** to **M6**, the latter five having chemically fixed torsion angles between the two phenyl rings, at the particular potential $E = -0.80$ V, where the gold surface is negatively charged (see the SI). The acquired spectra show an excellent signal-to-noise ratio. No Raman signals were obtained in the absence of the Au-NP-(55 nm) layer, as no local surface plasmons could be excited by the propagating optical wave on the atomically smooth Au(100) surface. On the other hand, the gap-mode spectra of all of the molecules studied revealed four dominant bands, such as those at 1083, 1200, 1283, and $\sim$1584 cm^{-1} for **M1** at $E = -0.80$ V. They are assigned to C$_{ring}$−S stretching, C−H in-plane bending $(-C_6H_4)$, C−C bridge stretching between the two phenyl rings, and aromatic tangential phenyl ring stretching (C=C).[13,21,34−36] Except for the band at 1584 cm^{-1}, the band positions shifted toward slightly higher values $(2-3$ cm^{-1} V$^{-1})$ as the potential became more negative. Their intensities increased until the onset of reductive desorption of the organic monolayer at $E < -1.10$ V.[32] The increase in intensity is tentatively attributed to the enhanced electromagnetic coupling between the Au-NP(55 nm) layer and the increasingly more negatively charged surface (see the SI).

Of particular interest are the bands at $\sim$1580 cm^{-1} (tangential C=C stretch in the two phenyl rings) and $\sim$1081 cm^{-1} (C$_{ring}$−S stretch). The intensity of the former depends on the conjugation of the two phenyl rings[16] and is therefore directly related to the torsion angle between the planes of the rings. On the other hand, the nature and intensity of the C$_{ring}$−S band is not related to conjugation and torsion angle. Consequently, we used this band as an internal standard. The ratio of the integrated intensities, $I_{C=C}/I_{C_{ring}−S}$, could be chosen as a measure of the interplanar torsion angle of the 4,4′-BPDT system under investigation. Figure 3A depicts $I_{C=C}/I_{C_{ring}−S}$ for **M1** as a function of the applied potential. The ratio increases rather slowly until $E \approx -0.60$ V, and subsequently at a more negatively charged surface (c.f. SI), the ratio increased more rapidly until desorption of the thiol occurred (solid circles). A similar trend was observed when the potential was scanned in the reverse direction from -1.10 to 0.0 V (open circles). From this we conclude that the torsion angle of **M1** changed reversibly with the applied
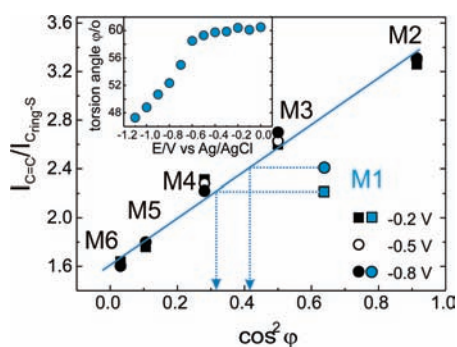
Figure 4. Plot of $I_{C=C}/I_{C_{ring}-S}$ vs $\cos^2 \varphi$ for **M1**−**6**.

potential, i.e. we observed a conformational change within the nanojunctions of the Au(100)|**M1**|Au-NP(55 nm) sandwich architecture in situ upon "electrolyte gating". Furthermore, we found that the $I_{C=C}/I_{C_{ring}-S}$ ratios for **M2**−**M6** were rather insensitive to the electrode potential (Figure 3B), indicating that the alkyl chains of various lengths bridging the 2 and 2′ positions fix the torsion angle under in situ electrochemical conditions. Comparing the data for **M1** with those obtained for **M2**−**M6** therefore provides a direct measure of the potential dependence of the torsion angle between the phenyl rings in **M1**, as determined using the relationship between φ and the $I_{C=C}/I_{C_{ring}-S}$ ratio.

Figure 4 depicts the relationship of the intensity ratio and $\cos^2 \varphi$ based on the data acquired for the six molecules at the representative potentials −0.20, −0.50, and −0.80 V. The $\cos^2 \varphi$ representation was chosen because theoretical studies indicated that the orbital overlap of adjacent π systems correlates with $\cos \varphi$ and that the electron transmission is proportional to $\cos^2 \varphi$.[29,37,38] A linear dependence is clearly observed for **M2**−**M6**, as expressed by the linear fit $I_{C=C}/I_{C_{ring}-S} = A + B \cos^2 \varphi$ with $A = 1.63 \pm 0.03$, $B = 1.88 \pm 0.07$, and $\sigma = 0.99$. The fixed torsion angles of these five molecules were obtained from crystal structure data.[29,31] Using this linear relationship as an internal calibration, we estimate a potential-induced change in the time-averaged torsion angle[30] of **M1** from 63° for −0.10 V < E < −0.50 V to 47° at −1.10 V. This trend of the potential-dependent decrease in the torsion angle for **M1**, which leads to an increasing π−π coupling and consequently electron delocalization between the two phenyl rings, correlates with the increasing accumulation of negative charge on the Au(100) surface (see the SI).

A linear relationship was also reported for the conductances of single-molecule junctions formed between **M2**−**M6** and gold leads.[29] This fact demonstrates that both measured parameters (i.e., molecular conductance and $I_{C=C}/I_{C_{ring}-S}$) reflect the π−π coupling between the aromatic rings. In other words, the applied electrochemical gate field (Debye screening length $\approx$ 1 nm, which is comparable to the thickness of the molecular adlayer) in combination with in situ gap-mode Raman spectroscopy in an Au(100)|4,4′-BPDT|Au-NP(55 nm) sandwich geometry provides access to structure changes in nanojunctions with direct relevance to (single) molecule transport experiments and other potential applications in molecule-inspired nanoelectronics. We note that the assembly chosen in the above experiment leads to an electrostatic potential gradient between the top of the NP layer and the Au(100) single-crystal surface. However, in comparison with an electronic transport experiment, there is no net current (i.e., no steady-state charge flow through the molecule takes place).

In summary, in situ gap-mode Raman spectra were acquired in an electrochemical environment on a single-crystal gold electrode employing a Au(100)|4,4′-BPDT|Au-NP(55 nm) sandwich assembly. This geometry enabled an investigation of the influence of an applied electrochemical gate field on conformational changes in nanojunctions, such as the torsion angle (φ) of molecules. A linear correlation between the intensity ratio $I_{C=C}/I_{C_{ring}-S}$ and $\cos^2 \varphi$ in 4,4′-BPDT-type molecular junctions was established and subsequently utilized to estimate the dependence of the time-averaged torsion angle of the "flexible" molecule **M1** at different electrode potentials. The latter decreases as the potential (charge) becomes more negative, resulting in better π−π coupling, which correlates with an enhanced junction conductance. The demonstrated spectroelectrochemical strategy and the direct correlation of the spectroscopic results with (single) molecular conductance studies may guide the selection and elucidation of functional molecules for potential applications in novel nanodevices.

■ ASSOCIATED CONTENT

ⓢ Supporting Information. Experimental details, including sample preparation, SERS measurements, data processing information, and potential of zero total charge. This material is available free of charge via the Internet at http://pubs.acs.org.

■ AUTHOR INFORMATION

Corresponding Author
thomas.wandlowski@dcb.unibe.ch

■ ACKNOWLEDGMENT

■ REFERENCES

(1) Love, J. L.; Estroff, L. A.; Kriebel, J. K.; Nuzzo, R. G.; Whitesides, G. M. *Chem. Rev.* **2005**, *105*, 1103−1169.

(2) Buck, M. *Adv. Electrochem. Sci. Eng.* **2009**, *11*, 197−247.

(3) Cuevas, J. C.; Scheer, E. *Molecular Electronics: An Introduction to Theory and Experiment*; World Scientific: Singapore, 2010.

(4) Akkerman, H. B.; de Boer, B. *J. Phys.: Condens. Matter* **2008**, *20*, No. 013001.

(5) Heath, J. R. *Annu. Rev. Mater. Res.* **2009**, *39*, 1−23.

(6) Special issue on "Molecular Electronics": *Chimia* **2010**, *6*, 348−420.

(7) Salomon, A.; Cahen, D.; Lindsay, S.; Tomfohr, J.; Engelkes, V. B.; Frisbie, C. D. *Adv. Mater.* **2003**, *15*, 1881−1890.

(8) McCreery, R. L.; Bergren, A. J. *Adv. Mater.* **2009**, *21*, 4303−4322.

(9) Abad, J. M.; Gass, M.; Bleloch, A.; Schiffrin, D. J. *J. Am. Chem. Soc.* **2009**, *131*, 10229−10236.

(10) Smalley, J. F.; Sachs, S. B.; Chidsey, C. E. D.; Dudek, S. P.; Sikes, H. D.; Creager, S. E.; Yu, C. L.; Feldberg, S. W.; Newton, M. D. *J. Am. Chem. Soc.* **2004**, *126*, 14620−14630.

(11) Wang, W. Y.; Lee, T.; Kretzschmar, I.; Reed, M. A. *Nano Lett.* **2004**, *4*, 643−646.

(12) Yu, L. H.; Zangmeister, C. D.; Kushmerick, J. G. *Phys. Rev. Lett.* **2007**, *98*, No. 206803.

(13) Ioffe, Z.; Shamai, T.; Ophir, A.; Noy, G.; Yutsis, I.; Kfir, K.; Cheshnovsky, O.; Selzer, Y. *Nat. Nanotechnol.* **2008**, *3*, 727−732.

(14) Ward, D. R.; Halas, N. J.; Ciszek, J. W.; Tour, J. M.; Wu, Y.; Nordlander, P.; Natelson, D. *Nano Lett.* **2008**, *8*, 919–924.

(15) Tian, J. H.; Liu, B.; Li, X.; Yang, Z. L.; Ren, B.; Wu, S. T.; Tao, N.; Tian, Z. Q. *J. Am. Chem. Soc.* **2006**, *128*, 14748–14749.

(16) Liu, Z.; Wang, X.; Dai, K.; Jin, S.; Zeng, Z. C.; Zhuang, M. D.; Yang, Z. L.; Wu, D. Y.; Ren, B.; Tian, Z. Q. *J. Raman Spectrosc.* **2009**, *40*, 1400–1406.

(17) McCreery, R. L.; Viswanathan, U.; Kalakodimi, R. P.; Nowak, A. M. *Faraday Discuss.* **2006**, *131*, 33–43.

(18) Jaiswal, A.; Tavakoli, K. G.; Zou, S. Z. *Anal. Chem.* **2006**, *78*, 120–124.

(19) *Surface Enhanced Raman Scattering*; Kneipp, K., Moskovits, M., Kneipp, H., Eds.; Springer: Berlin, 2006.

(20) Zhou, Q.; Li, X. W.; Fan, Q.; Zhang, X. X.; Zheng, J. W. *Angew. Chem., Int. Ed.* **2006**, *45*, 3970–3973.

(21) Ikeda, K.; Fujimoto, N.; Uehara, H.; Uosaki, K. *Chem. Phys. Lett.* **2008**, *460*, 205–208.

(22) Park, W. H.; Kim, Z. H. *Nano Lett.* **2010**, *10*, 4040–4048.

(23) Haran, G. *Acc. Chem. Res.* **2010**, *43*, 1135–1143.

(24) Huang, Y. F.; Yin, N. N.; Wang, X.; Wu, D. Y.; Ren, B.; Tian, Z. Q. *Chem.—Eur. J.* **2010**, *16*, 1449–1453.

(25) Jung, U.; Müller, M.; Fujimoto, N.; Ikeda, K.; Uosaki, K.; Cornelissen, U.; Tuczek, F.; Bornholdt, C.; Zargarani, D.; Herges, R.; Magnussen, O. *J. Colloid Interface Sci.* **2010**, *341*, 366–375.

(26) Li, J. F.; Huang, Y. F.; Ding, Y.; Yang, Z. L.; Li, S. B.; Zhou, X. S.; Fan, F. R.; Zhang, W.; Zhou, Z. Y.; Wu, D. Y.; Ren, B.; Wang, Z. L.; Tian, Z. Q. *Nature* **2010**, *464*, 392–395.

(27) White, H. S.; Kittlesen, G. P.; Wrighton, M. S. *J. Am. Chem. Soc.* **1984**, *106*, 5375–5377.

(28) Venkataraman, L.; Klare, J. E.; Nuckolls, C.; Hybertsen, M. S.; Steigerwald, M. L. *Nature* **2006**, *442*, 904–907.

(29) Vonlanthen, D.; Mishchenko, A.; Elbing, M.; Neuburger, M.; Wandlowski, T.; Mayor, M. *Angew. Chem., Int. Ed.* **2009**, *48*, 8886–8890. Mishchenko, A.; Vonlanthen, D.; Meded, V.; Burkle, M.; Li, C.; Pobelov, I. V.; Bagrets, A.; Viljas, J. K.; Pauly, F.; Evers, F.; Mayor, M.; Wandlowski, T. *Nano Lett.* **2010**, *10*, 156–163.

(30) Mishchenko, A.; Zotti, L. A.; Vonlathen, D.; Bürkle, M.; Pauly, F.; Cuevas, J. C.; Mayor, M; Wandlowski, T. *J. Am. Chem. Soc.* **2011**, *133*, 184–187.

(31) Shaporenko, A.; Elbing, M.; Blaszczyk, A.; von Hänisch, C.; Mayor, M.; Zharnikov, M. *J. Phys. Chem. B* **2006**, *110*, 4307–4317.

(32) Azzam, W.; Wehner, B. I.; Fischer, R. A.; Terfort, A.; Wöll, C. *Langmuir* **2002**, *18*, 7766–7769.

(33) Frens, G. *Nat. Phys. Sci.* **1973**, *241*, 20–22.

(34) Han, S. W.; Lee, S. J.; Kim, K. *Langmuir* **2001**, *17*, 6981–6987.

(35) Fletcher, M. C.; Vivoni, A.; Moore, M. M.; Lui, J.; Caldwell, J.; Prokes, S. M.; Glembocki, O.; Hosten, C. M. *Surf. Sci.* **2008**, *602*, 1614–1621.

(36) Ge, J. J.; Li, C. Y.; Xue, G.; Mann, I. K.; Zhang, D.; Wang, S. Y.; Harris, F. W.; Cheng, S. Z.; Hong, S. C.; Zhuang, X. W.; Shen, Y. R. *J. Am. Chem. Soc.* **2001**, *123*, 5768–5776.

(37) Woitellier, S.; Launay, J. P.; Joachim, C. *Chem. Phys.* **1989**, *131*, 481–488.

(38) Nitzan, A. *J. Phys. Chem. A* **2001**, *105*, 2677–2679.